BJP British Journal of Pharmacology

DOI:10.1111/bph.13153
www.brjpharmacol.org

RESEARCH PAPER

PKPD modelling to predict altered disposition of 1α,25-dihydroxyvitamin D_3 in mice due to dose-dependent regulation of CYP27B1 on synthesis and CYP24A1 on degradation

Holly P Quach[1], Qi J Yang[1], Edwin C Chow[1], Donald E Mager[2], Stacie Y Hoi[1] and K Sandy Pang[1]

[1]*Department of Pharmaceutical Sciences, Leslie Dan Faculty of Pharmacy, University of Toronto, Toronto, Ontario, Canada, and* [2]*Department of Pharmaceutical Sciences, University at Buffalo, State University of New York, Buffalo, NY, USA*

Correspondence
K. Sandy Pang, Leslie Dan Faculty of Pharmacy, University of Toronto, 144 College Street, Toronto, ON, M5S 3M2 Canada.
E-mail: ks.pang@utoronto.ca

Received
16 October 2014
Revised
3 February 2015
Accepted
25 March 2015

BACKGROUND AND PURPOSE

Concentrations of 1α,25-dihydroxyvitamin D_3 [1,25$(OH)_2D_3$], the active ligand of the vitamin D receptor, are tightly regulated by CYP27B1 for synthesis and CYP24A1 for degradation. However, the dose-dependent pharmacokinetic (PK)-pharmacodynamic (PD) relationship between these enzymes and 1,25$(OH)_2D_3$ concentrations has not been characterized.

EXPERIMENTAL APPROACH

The pharmacokinetics of 1,25$(OH)_2D_3$ were evaluated after administration of single (2, 60 and 120 pmol) and repeated (2 and 120 pmol q2d ×3) i.v. doses to male C57BL/6 mice. mRNA expression of CYP27B1 and CYP24A1 was examined by quantitative PCR and 1,25$(OH)_2D_3$ concentrations were determined by enzyme immunoassay.

KEY RESULTS

CYP27B1 and CYP24A1 changes were absent for the 2 pmol dose and biexponential decay profiles showed progressively shorter terminal half-lives with increasing doses. Fitting with a two-compartment model revealed decreasing net synthesis rates and increasing total clearances with dose, consistent with a dose-dependent down-regulation of renal CYP27B1 and the induction of renal/intestinal CYP24A1 mRNA expression. Upon incorporation of PD parameters for inhibition of CYP27B1 and induction of CYP24A1 to the simple two-compartment model, fitting was significantly improved. Moreover, fitted estimates for the 2 pmol dose, together with the PD parameters as modifiers, were able to predict profiles reasonably well for the higher (60 and 120 pmol) doses. Lastly, an indirect response model, which considered the synthesis and degradation of enzymes, adequately described the PK and PD profiles.

CONCLUSIONS AND IMPLICATIONS

The unique PK of exogenously administered 1,25$(OH)_2D_3$ led to changes in PD of CYP27B1 and CYP24A1, which hastened the clearance of 1,25$(OH)_2D_3$.

Abbreviations

AIC, Akaike information criterion; AUC, area under the plasma concentration time curve; CL, clearance; DBP, vitamin D binding protein; k, rate constant; PD, pharmacodynamic; PK, pharmacokinetic; PTH, parathyroid hormone; qPCR, quantitative real-time PCR; R_{syn}, net rate of synthesis; V_1, volume of central compartment; V_{ss}, volume of distribution at steady state; WSSR, weighted sum of square residuals; $1,25(OH)_2D_3$, 1α,25-dihydroxyvitamin D_3; $25(OH)D_3$, 25-hydroxyvitamin D_3

Tables of Links

TARGETS	
Ion channels[a]	**Enzymes**[c]
TRPV5	CYP24A1
TRPV6	CYP27A1
Nuclear hormone receptors[b]	CYP27B1
Vitamin D receptor	CYP2R1

LIGANDS
1α,25-dihydroxyvitamin D_3
25-hydroxyvitamin D_3
PTH
Vitamin D

These Tables list key protein targets and ligands in this article which are hyperlinked to corresponding entries in http://www.guidetopharmacology.org, the common portal for data from the IUPHAR/BPS Guide to PHARMACOLOGY (Pawson *et al.*, 2014) and are permanently archived in the Concise Guideto PHARMACOLOGY 2013/14 ([a,b,c]Alexander *et al.*, 2013a,b,c).

Introduction

Vitamin D, formed from 7-dehydrocholesterol in skin upon exposure to sunlight, is metabolized by CYP2R1 and CYP27A1 in liver to its major circulating form, 25-hydroxyvitamin D_3 [$25(OH)D_3$]. This relatively inactive metabolite is transported by the vitamin D binding protein (DBP) for activation by 1α-hydroxylase (CYP27B1) in the kidney to form the active ligand of the vitamin D receptor, 1α,25-dihydroxyvitamin D_3 [$1,25(OH)_2D_3$] (Jones *et al.*, 1998). A major physiological role of $1,25(OH)_2D_3$ is to regulate plasma calcium concentrations through the calcium ion channels, TRPV5 and TRPV6, in the kidney and intestine (den Dekker *et al.*, 2003) and the calcium-sensing receptor (Carrillo-Lopez *et al.*, 2008). Continuous bone turnover, including resorption of existing bone and deposition of new bone, is another process that is stimulated by $1,25(OH)_2D_3$ and the parathyroid hormone (PTH) (Jones *et al.*, 1998; Hoenderop *et al.*, 2005).

Calcium and $1,25(OH)_2D_3$ homeostasis is tightly controlled by $1,25(OH)_2D_3$, calcium and PTH (Shinki *et al.*, 1992; Masuda *et al.*, 2005; Turunen *et al.*, 2007). Plasma $1,25(OH)_2D_3$ concentrations are regulated by two major enzymes: CYP27B1 for synthesis and CYP24A1 for degradation. CYP27B1, expressed predominantly in the kidney, responds positively to PTH at low plasma calcium concentrations (Shinki *et al.*, 1992), but is down-regulated by high concentrations of $1,25(OH)_2D_3$ (Brenza and DeLuca, 2000; Turunen *et al.*, 2007). CYP24A1, distributed abundantly in the kidney and intestine, is responsible for the metabolism of $25(OH)D_3$ to 24,25-dihydroxyvitamin D_3 and $1,25(OH)_2D_3$ to 1α,24,25-trihydroxyvitamin D_3 (Holick *et al.*, 1972; Kumar *et al.*, 1978; Halloran and Castro, 1989). Because elevated concentrations of $1,25(OH)_2D_3$ are known to cause hypercalcaemia (Jones *et al.*, 1987; Makin *et al.*, 1989), CYP24A1 expression in the kidney is up-regulated as a feedback mechanism to increase $1,25(OH)_2D_3$ catabolism and reduce $1,25(OH)_2D_3$ and $25(OH)D_3$ stores (Clements *et al.*, 1992). In contrast, intestinal CYP24A1 is regulated by $1,25(OH)_2D_3$ and not PTH (Henry, 2001), suggesting that the induction of intestinal CYP24A1 is an acute response to the vitamin D receptor (Akeno *et al.*, 1994).

Pharmacokinetic (PK) studies of $1,25(OH)_2D_3$ are challenging due to assay sensitivity in measuring low $1,25(OH)_2D_3$ concentrations and studies in rodents are further hampered by the limited plasma volume for sampling. Masuda *et al.* (2005) examined the decay of radiolabelled $1,25(OH)_2D_3$ over 96 h in *CYP24A1(+/–)* and *CYP24A1(–/–)* mice, confirming that CYP24A1 is the major enzyme involved in the metabolism of $1,25(OH)_2D_3$. *CYP24A1(–/–)* mice exhibited a longer $t_{1/2}$ compared with *CYP24A1(+/–)* mice. In a phase I clinical trial, where 2 to 10 μg $1,25(OH)_2D_3$ was administered s.c., the derived $t_{1/2}$ proved to be ill-defined due to inadequate sampling over 12 h (Smith *et al.*, 1999). In a human study in which prolonged sampling was conducted following p.o. and i.v. doses of 4 μg $1,25(OH)_2D_3$, a $t_{1/2}$ of 26 h was observed, along with a plasma clearance ($dose/AUC_\infty$) of 0.17 $mL \cdot min^{-1} \cdot kg^{-1}$ and bioavailability of 0.71 after 72 h of sampling (Brandi *et al.*, 2002). C3H/HeJ mice treated with 0.125 or 0.5 μg $1,25(OH)_2D_3$ i.p., with sampling up to 24 h, produced an apparent clearance ($dose/AUC_{0\rightarrow24}$), but a debatable terminal $t_{1/2}$ due to limited sampling (Muindi *et al.*, 2004). Chow *et al.* (2013) reported an apparent terminal $t_{1/2}$ of 6.8 h after sampling for 48 h in mice treated with 0.05 μg $1,25(OH)_2D_3$ i.p. and showed that both plasma and tissue $1,25(OH)_2D_3$ concentrations fell below basal levels at 24 h due to the induction of CYP24A1. None of these studies provided an in-depth interpretation of the PK when describing the net rate of synthesis (R_{syn}) of endogenous $1,25(OH)_2D_3$ nor accounted for pharmacodynamic (PD) changes on the inhibition of CYP27B1 or induction of CYP24A1.

In this study, we examined the PD changes driven by $1,25(OH)_2D_3$ PK in relation to basal concentrations of

1,25(OH)$_2$D$_3$. Single and repeated i.v. doses were administered to mice to appraise the dose- and time-dependent PK of 1,25(OH)$_2$D$_3$. Fitting with a simple two-compartment model yielded a decreasing R_{syn} and increasing total plasma clearance (CL_{total}), observations consistent with the inhibition of CYP27B1 and induction of CYP24A1 with dose. Inclusion of parameters associated with PD changes in mRNA expression for the down-regulation of CYP27B1 and the induction of CYP24A1, obtained upon regression of mRNA expression fold change (FC) of enzymes in tissue versus 1,25(OH)$_2$D$_3$ plasma concentration, significantly improved model fitting criteria. Lastly, an indirect response model was able to provide similar parameters as the PD-linked model and predicted the temporal PK and PD data for the different doses administered. The composite data show that changes in the PD of CYP27B1 and CYP24A1 with increasing 1,25(OH)$_2$D$_3$ doses resulted in altered PK of 1,25(OH)$_2$D$_3$.

Methods

Pharmacokinetic study

The concentration of 1,25(OH)$_2$D$_3$ in anhydrous ethanol was assayed spectrophotometrically at 265 nm (UV-1700, Shimadzu Scientific Instruments, Mandel Scientific, Guelph, Ontario, Canada) and diluted with sterile 0.9% saline containing 1% ethanol. Male C57BL/6 mice (8 weeks old), weighing 25.5 ± 1.6 g (mean ± SD), were purchased from Charles River Canada (Saint-Constant, Quebec, Canada). Mice were given water and food *ad libitum* and maintained under a 12:12 h light and dark cycle in accordance with approved protocols by the Animal Care and Use Committee at the University of Toronto. All studies involving animals are reported in accordance with the ARRIVE guidelines for reporting experiments involving animals (Kilkenny *et al.*, 2010; McGrath *et al.*, 2010). A total of 130 mice were used in the experiments described. Mice were randomly assigned to treatment with single (0, 2, 60 or 120 pmol) or repeated (0, 2 or 120 pmol q2d ×3) i.v. doses of 1,25(OH)$_2$D$_3$ on days 0, 2 and 4 at 0900 h. Serial blood sampling from the saphenous vein was performed at 1, 5, 15, 30 or 60 min. Thereafter, mice were anaesthetized with ketamine and xylazine i.p. (150 and 10 mg·kg^{-1} respectively) before blood collection by cardiac puncture with a 1 mL syringe-23G 3/4″ needle set that was pre-rinsed with heparin (1000 IU·mL^{-1}). The depth of anaesthesia was assessed by monitoring the heart rate and pedal reflex. Tissues were harvested at each sampling point (3, 6, 9, 12, 24 and 48 h) from the treated mice (n = 3–4 per time point). For the vehicle-treated group (n = 9), sampling was conducted at 0 h on days 0 and 4 and averaged, as described previously (Chow *et al.*, 2013), to provide basal concentrations. Plasma was obtained by centrifugation of blood at 3000× g for 10 min. After flushing the lower vena cava with ice-cold saline, the kidneys and ileum (6 cm proximal to the ileocecal junction) were removed over ice as outlined previously (Chow *et al.*, 2011). Samples were snap-frozen in liquid nitrogen and stored at –80°C.

Plasma 1,25(OH)2D$_3$ analysis

Plasma 1,25(OH)$_2$D$_3$ concentrations were measured by enzyme immunoassay (EIA) (Chow *et al.*, 2013).

Quantitative real-time PCR (qPCR)

Total RNA, obtained from kidney tissues and scraped ileal enterocytes, was extracted using the TRIzol extraction method (Sigma-Aldrich, Mississauga, Ontario, Canada) in accordance with the manufacturer's protocol, with modifications (Chow *et al.*, 2011). A total of 1.5 µg of cDNA was synthesized from RNA using the high capacity cDNA reverse transcription kit (Applied Biosystems® by Life Technologies, Burlington, Ontario, Canada) and qPCR was performed with SYBR Green detection system. Kidney and intestinal mRNA data were normalized to cyclophilin and villin, respectively, for calculation of the relative change in gene expression (Chow *et al.*, 2009).

PK and PD analysis

Non-compartmental analysis. The AUC from 0 to 48 h ($AUC_{0\rightarrow48h}$) was estimated by the trapezoidal rule. The extrapolated area from the last datum point to time infinity ($AUC_{48h\rightarrow\infty}$) was calculated upon dividing the measured plasma concentration, C_{48h}, by the terminal slope (β). Other parameters included: $t_{1/2\beta}$ or terminal half-life, estimated from data between 6 and 48 h and calculated as 0.693/β, and CL_{total}, estimated as dose/AUC_∞.

Estimation of PD parameters for inhibition and induction. The mRNA expression of renal CYP27B1 and renal and ileal CYP24A1 was normalized to basal levels (vehicle-treated mice) and the FC was plotted against the plasma 1,25(OH)$_2$D$_3$ concentration. For CYP27B1, the inhibition function or FC of CYP27B1 ($CYP27B1_{FC}$) was

$$CYP27B1_{FC} = \left(1 - \frac{I_{max}C_p}{IC_{50} + C_p}\right) \quad (1)$$

For CYP24A1, the induction function or FC of CYP24A1 ($CYP24A1_{FC}$) was

$$CYP24A1_{FC} = \left(1 + \frac{E_{max}C_p}{EC_{50} + C_p}\right) \quad (2)$$

with C_p as the plasma 1,25(OH)$_2$D$_3$ concentration, the maximal FC as I_{max} and E_{max} for inhibition and induction factors, and IC_{50} and EC_{50} as the plasma concentrations that result in 50% of I_{max} and E_{max} (Mager *et al.*, 2009). The E_{max}, EC_{50}, I_{max} and IC_{50} estimates were obtained upon non-linear regression of single and repeated dose and combined data from all doses with Equations 1 and 2 using Scientist® (version 2.0; Micromath, St. Louis, Missouri, USA).

Fitting without consideration of PD: simple two-compartment model. Fitting was conducted with Scientist with appropriate weighting schemes (unity, 1/observation and 1/observation^2) or with ADAPT5 (version 5; Biomedical Simulations Resource, University of Southern California, Los Angeles, California, USA). Assuming stationary kinetics and dynamics, we estimated the volume of the central compartment (V_1), net synthesis rate (R_{syn}) controlled by CYP27B1 and the micro-rate constants (k_{12}, k_{21}, k_{10}) during the first 48 h of sampling. The fit for each of the single 2, 60 or 120 pmol dose levels was obtained with a simple two-compartment model (Figure 1A and equations in Appendix A). The steady-state volume of distribution (V_{ss}) was estimated as V_1·(1 +

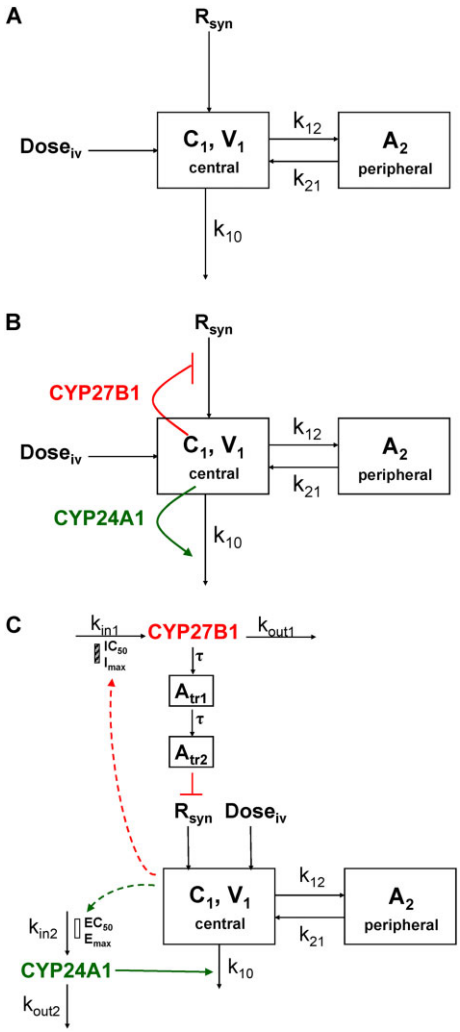

Figure 1

Fitting of $1,25(OH)_2D_3$ data using (A) a simple two-compartment model, (B) a PD-linked model and (C) an indirect response model. For the compartmental models, it is assumed that synthesis and elimination of $1,25(OH)_2D_3$ are occurring from the central compartment.

k_{12}/k_{21}). Values of k_{12} for the 60 and 120 pmol doses are expressed as multiples of k_{12}, relative to the 2 pmol dose, for the combined fit of all data (1.5× and 5.7× the k_{12} value of the 2 pmol dose). Parameter estimates obtained from the single doses were used as initial estimates for the combined fit to all data upon repeated dosing.

Integrated PKPD model. Parameters governing changes in CYP27B1 and CYP24A1 expression were incorporated into a two-compartment model (Figure 1B and Appendix B) to modify R_{syn} and k_{10}. Based on the assumption that there was no down-regulation of CYP27B1 nor induction of CYP24A1 for the 2 pmol dose, fitted parameters for this dose (V_1, k_{12}, k_{21}, R_{syn} and k_{10}) from the two-compartment model were used as initial estimates, together with averaged estimates of I_{max}, IC_{50}, E_{max} and EC_{50} (Table 3), for combined fitting of data for the first doses (2, 60 and 120 pmol) and data from all doses. Fitting was repeated upon addition of scaling factors, then Hill coefficients (Appendix B). Again, k_{12} values for the 60 and 120 pmol doses were scaled to account for possible changes in the distribution of $1,25(OH)_2D_3$ in the simultaneous fits. The PD-linked models were compared with the simple two-compartment model using the F-test (Boxenbaum *et al.*, 1974).

Fitting with the indirect response model. The indirect response model (Figure 1C), which describes an indirect mechanism of action and incorporates transit compartments ($A_{transit1}$ and $A_{transit2}$) containing a time-delay function (τ) (Appendix C), relates temporal differences between drug concentrations and responses (Mager *et al.*, 2003). The indirect response model was used to explain the time delay for the CYP27B1 effects, assuming CYP27B1 is indirectly stimulated by PTH-induced activation of the vitamin D receptor. Similar to the PD-linked model, scaling factors and Hill coefficients were incorporated for fitting purposes.

Statistical analysis. The mRNA data are expressed as mean ± SEM. One-way ANOVA and a *post hoc* Tukey honest significant difference test were used to evaluate differences between mean mRNA expression of groups at each time point using GraphPad Prism Software (version 6; GraphPad Software Inc., La Jolla, California, USA). The goodness of fit was appraised by the weighted sum of square residuals (WSSR), Akaike information criterion (AIC), and SD of the parameter estimate, while the F-test was used for comparing the models. Significance was defined as $P < 0.05$.

Materials

$1,25(OH)_2D_3$ in powder form was obtained from Sigma-Aldrich. The EIA kit (Cat# AC-62F1) for $1,25(OH)_2D_3$ measurements was manufactured by Immunodiagnostics Systems Inc. (Scottsdale, Arizona, USA) and purchased from Inter Medico (Markham, Ontario, Canada). All other reagents were obtained from Sigma-Aldrich and Fisher Scientific (Mississauga, Ontario, Canada).

Results

Dose-dependent PK of $1,25(OH)_2D_3$

$1,25(OH)_2D_3$ concentrations for the 60 and 120 pmol doses fell below basal values (187 ± 48.5 pM) by 24 h whereas those for the 2 pmol dose remained relatively unchanged. Plasma $1,25(OH)_2D_3$ concentrations decayed biexponentially at each dose level (Figure 2). There was a prolonged $t_{1/2\beta}$ (36.7 h) for the lowest dose and a dramatically shorter $t_{1/2\beta}$ (~6 h) for higher doses (Table 1). Non-compartmental values of AUC_∞/dose decreased with increasing dose, yielding greater clearance values at higher doses. CL_{total} increased from 0.1 to 2.0 $mL \cdot min^{-1} \cdot kg^{-1}$ (Table 1), an observation compatible with induction of CYP24A1 for the metabolism of $1,25(OH)_2D_3$.

For the simple two-compartment model that contained R_{syn} for $1,25(OH)_2D_3$ formation from its vitamin D precursors, fits to the single dose data individually revealed a decreasing R_{syn} and an increasing k_{10} with increasing dose (Figure 2A;

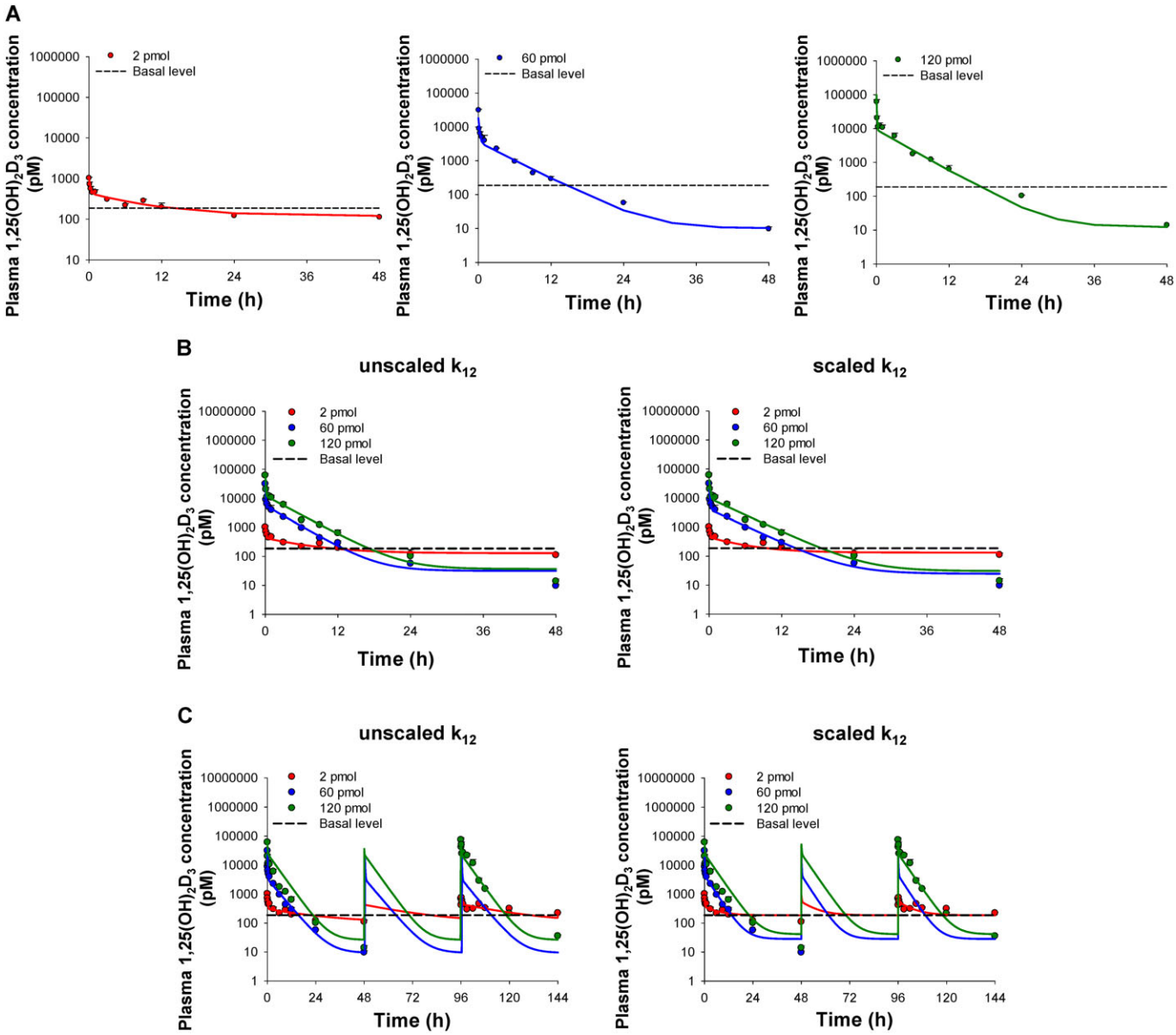

Figure 2

Plasma 1,25(OH)$_2$D$_3$ concentrations after i.v. administration of 2, 60 and 120 pmol doses versus basal levels. The two-compartment model was used to fit the 1,25(OH)$_2$D$_3$ data for each single 2, 60 or 120 pmol dose (A) individually, (B) combined fit of data for the first doses, with unscaled or scaled k_{12}, and (C) combined fit of data for all doses, with unscaled or scaled k_{12}. Observed plasma 1,25(OH)$_2$D$_3$ concentrations are shown as mean ± SEM (n = 3–4 different mice) with fitted values shown as a solid line. Data for vehicle-treated mice (basal level) were averaged and joined by the dashed line (n = 9).

Table 2). Furthermore, fitted values of k_{12} and V_{ss} increased with dose, suggesting a larger distribution volume with increasing dose levels. These distributional changes could not be explained by a saturation of protein binding sites as the 5 μM concentration of DBP in plasma (Chun, 2012) greatly exceeds the plasma 1,25(OH)$_2$D$_3$ concentrations from i.v. dosing. We then performed combined fitting of all data from the first doses and compared the parameter estimates obtained to those from individual fits. Accommodation of the changing k_{12} was accomplished by scaling k_{12} with dose (Table 2; Appendix A). The model predicted the data for the first dose well, whether or not k_{12} was scaled (Figure 2B). For the two-compartment model, the fitted k_{12} value for the 2 pmol dose (2.77 ± 1.42 h^{-1}), obtained from the individual fit of the 2 pmol data (Figure 2A), was about half that from forced fitting of data from the first doses (4.15 ± 1.23 h^{-1}) and with scaling of k_{12} (Table 2). For fitting of the first and repeated doses, the fit to the third 120 pmol dose was better than the fit to the first dose, with or without k_{12} scaled (Figure 2C). For the forced fit to all data from single and repeated dosing, the averaged value of the fitted k_{12} was halved when k_{12} was scaled, k_{21} and k_{10} were lower and V_1 and

V_{ss} were higher (Table 2). The WSSR was smaller with scaled k_{12} (although the AICs were similar), suggesting that scaling of k_{12} was an improvement (Table 2). The lack of a significant improvement in the forced fit for scaled k_{12} versus unscaled k_{12} was likely due to the inability of this model to account for the dose-dependent nature of R_{syn} and k_{10}.

CYP27B1 and CYP24A1 mRNA expression

The mRNA expression of the synthetic enzyme in kidney and degradation enzyme in intestine and kidney also displayed dose-dependent changes (Figure 3). For the 2 pmol single dose, there was an absence of any notable trend for the mRNA expression of renal CYP27B1 or renal and ileal CYP24A1, as levels remained relatively unchanged in relation to basal values (Figure 3, left panel). Furthermore, hypercalcaemia was not observed for the low dose (data not shown). Thus, the R_{syn} value obtained for the 2 pmol dose should represent the net synthesis rate of endogenous $1,25(OH)_2D_3$ formation from its vitamin D precursors. In contrast, markedly lower CYP27B1 mRNA expression at 9 h after $1,25(OH)_2D_3$ administration was noted with higher doses, wherein levels fell and remained below basal levels. Maximal induction of renal CYP24A1 expression occurred at 6–9 h and was sustained until 48 h. In ileum, maximal induction of CYP24A1 mRNA expression occurred at 3 h following the 60 pmol dose and at 6 h following the 120 pmol dose (Figure 3, left panel). Repeated administration of 120 pmol $1,25(OH)_2D_3$ led to a greater down-regulation (CYP27B1) and induction (CYP24A1) of renal mRNA levels when compared with the single dose and a similar pattern was observed for ileal CYP24A1 mRNA expression (Figure 3, right panel).

PD response versus concentration curves

Figure 4 shows the concentration-response relationship for FC of renal CYP27B1 and CYP24A1 and intestinal CYP24A1 mRNA expression in mice receiving single (2, 60 and 120 pmol) and repeated (2 and 120 pmol) doses of $1,25(OH)_2D_3$. A plateau was reached for CYP27B1 and CYP24A1 within the dose range and FC for CYP27B1 down-regulation or CYP24A1 induction remained constant at $1,25(OH)_2D_3$ concentrations >5000 pM. Upon fitting of Equation 1, a threefold increase in I_{max} was observed after repeated dosing (Table 3; Figure 4A), although the fitted IC_{50} values were similar for the single and repeated doses. Composite I_{max} and IC_{50} values were also obtained upon regression of pooled data from the first and repeated doses with Equation 1 and these values were similar to those obtained for the repeated third dose (Table 3). Estimated E_{max} values (expressed over basal level) obtained for CYP24A1 (Equation 2) for the first and the third doses were virtually identical (Figure 4B,C), whereas EC_{50} values for both renal and intestinal CYP24A1 increased significantly upon repeated dosing compared with that for the first dose (Table 3). Values for E_{max} and EC_{50} for the pooled data were similar to those for the third dose. For fitting of Equation B1 of Appendix B, the E_{max} values obtained

Table 1

Non-compartmental pharmacokinetic parameters following administration of first doses of $1,25(OH)_2D_3$ to mice

	Dose (pmol)		
	2	60	120
$t_{1/2\beta}$ (h)[a]	36.7	6.6	6.0
AUC_∞ (pM·h)[b]	14 900	24 500	57 200
AUC_∞/dose (h·L^{-1})	7 460	409	477
CL_{total} (mL·min^{-1}·kg^{-1})[c]	0.112	2.04	1.75

[a]$t_{1/2\beta}$ was calculated as 0.693/β, where β is the terminal slope of ln(concentration) versus time data between 6 and 48 h.
[b]AUC_∞ was determined as ($AUC_{0\to48}$ + C_{last}/β) and $AUC_{0\to48}$ was estimated by the trapezoidal rule.
[c]CL_{total} was estimated as dose/AUC_∞.

Table 2

Fitted pharmacokinetic parameters for first doses of $1,25(OH)_2D_3$ according to the simple two-compartment model

	Individual fitting to first dose			Forced fitting to first doses	
	2 pmol	60 pmol	120 pmol	2, 60 and 120 pmol k_{12} unscaled	2, 60 and 120 pmol k_{12} scaled
k_{12} (h^{-1})	2.77 ± 1.42[c]	4.17 ± 3.57	15.8 ± 4.36	10.8 ± 4.67	4.15 ± 1.23
k_{21} (h^{-1})	2.15 ± 1.14	1.41 ± 0.74	2.09 ± 0.40	2.93 ± 0.10	1.89 ± 0.49
k_{10} (h^{-1})	0.27 ± 1.10	0.93 ± 0.44	2.21 ± 0.71	1.11 ± 0.71	0.75 ± 0.37
V_1 (mL·kg^{-1})	112 ± 17.0	167 ± 81.5	61.5 ± 21.0	72.0 ± 1.6	117 ± 10.5
V_{ss} (mL·kg^{-1})[a]	255	659	526	337	409
R_{syn} (fmol·h^{-1})[b]	71.9 ± 39.8	31.1 ± 10.8	32.6 ± 5.91	85.5 ± 4.78	81.6 ± 16.4
WSSR				9.05	5.73
AIC				494	523

[a]V_{ss} was calculated as V_1 + V_2, where V_2, peripheral compartment = V_1 (k_{12}/k_{21}).
[b]R_{syn} initial estimate (49.6 fmol·h^{-1}) was obtained from Hsu *et al.* (1987).
[c]SD of parameter estimate.

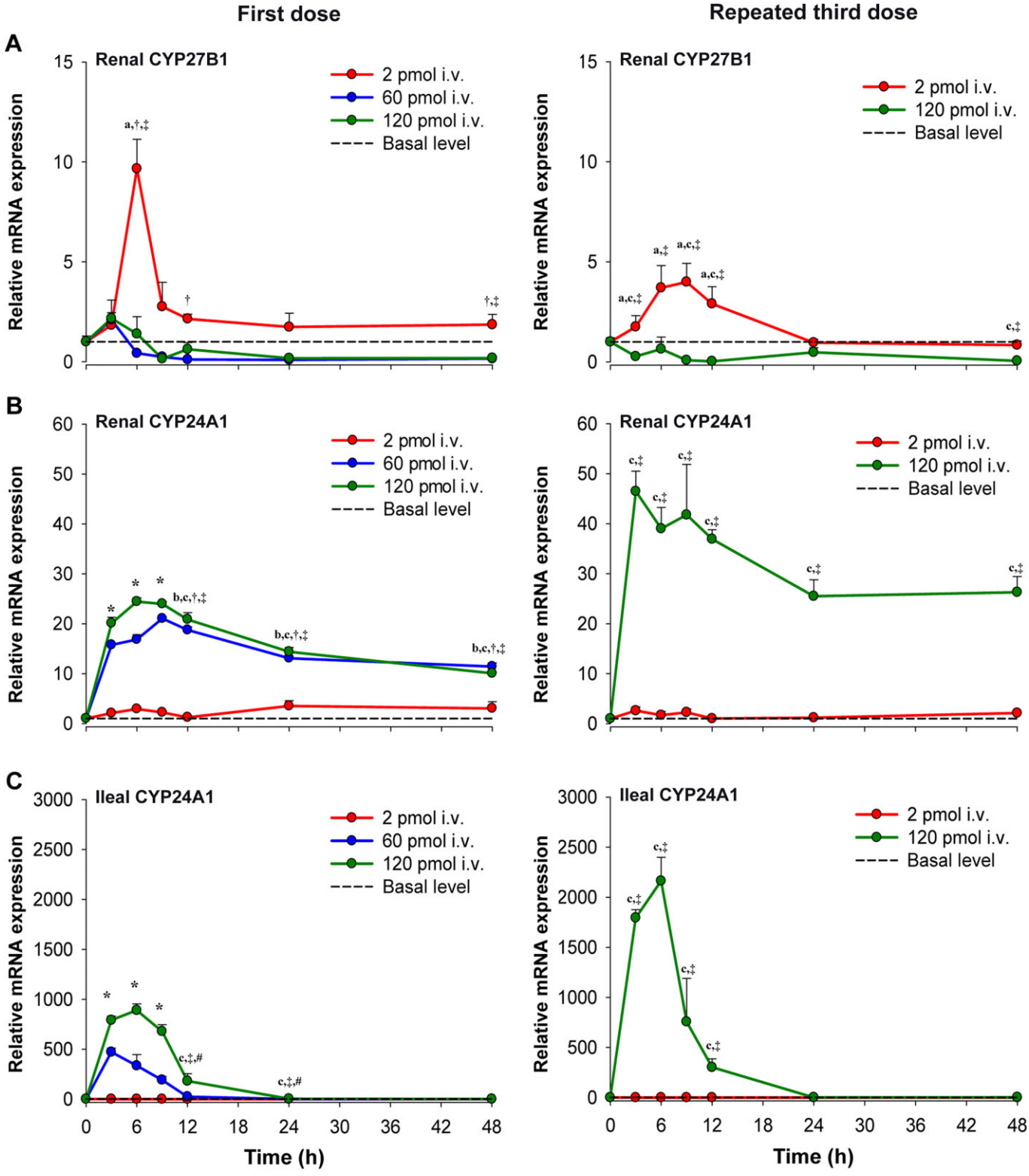

Figure 3

Relative mRNA expression for synthesis and degradation enzymes following single or repeated i.v. administration of 1,25(OH)$_2$D$_3$. (A) Renal CYP27B1 mRNA expression is reduced by both single and repeated administration of 60 and 120 pmol 1,25(OH)$_2$D$_3$. (B) Renal and (C) ileal CYP24A1 mRNA expression are induced by 1,25(OH)$_2$D$_3$ in a dose-dependent manner for single and repeated dosing. Data for vehicle-treated mice (basal level) were averaged and joined by the dashed line (n = 9), whereas data for treated mice are mean ± SEM and joined by a solid line (n = 3–4 different mice). Significant differences between groups were denoted by: [a]basal level versus 2 pmol; [b]basal level versus 60 pmol; [c]basal level versus 120 pmol; [†]2 pmol versus 60 pmol; [‡]2 pmol versus 120 pmol; [#]60 pmol versus 120 pmol; *all groups except basal level versus 2 pmol.

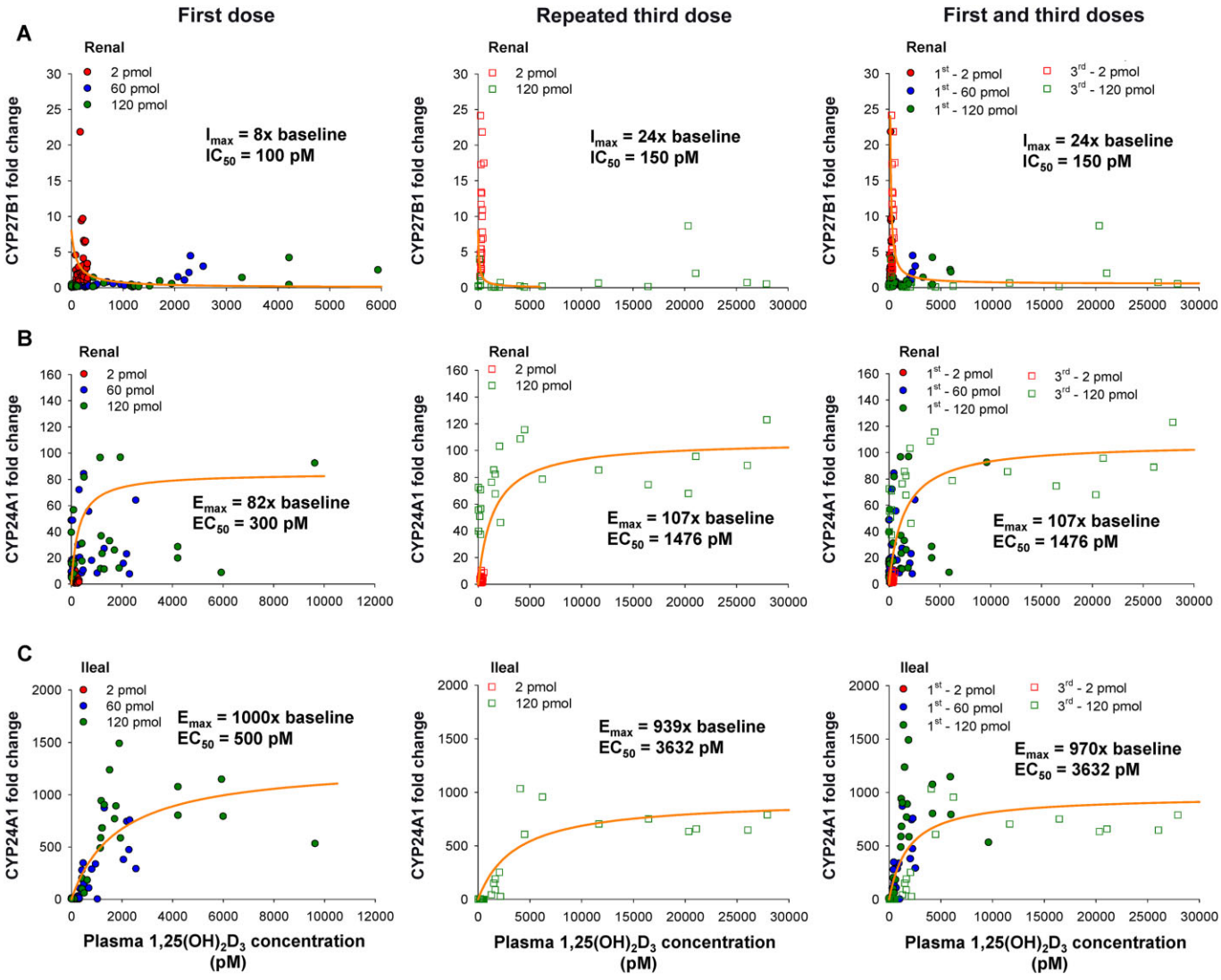

Figure 4

Inhibition of CYP27B1 and induction of CYP24A1 by $1,25(OH)_2D_3$. Plots of renal CYP27B1 and renal and intestinal CYP24A1 mRNA FC versus plasma concentration of $1,25(OH)_2D_3$ following first or third dose of 2, 60 and 120 pmol, with equations for inhibition $CYP27B1_{FC} = \left(1 - \frac{I_{max} C_p}{IC_{50} + C_p}\right)$ and induction $CYP24A1_{FC} = \left(1 + \frac{E_{max} C_p}{EC_{50} + C_p}\right)$.

Table 3

Pharmacodynamic parameters estimated from CYP27B1 or CYP24A1 fold change versus plasma $1,25(OH)_2D_3$ concentration

	Renal CYP27B1		Renal CYP24A1		Ileal CYP24A1	
	I_{max}[a]	IC_{50} (pM)	E_{max}[a]	EC_{50} (pM)	E_{max}[a]	EC_{50} (pM)
For first dose	8 ± 2[b]	100 ± 9	82 ± 19	300 ± 23	1000 ± 129	500 ± 62
For repeated third dose	24 ± 2	150 ± 15	107 ± 16	1480 ± 90	939 ± 126	3630 ± 220
For first and third doses	24 ± 4	150 ± 24	107 ± 19	1480 ± 189	970 ± 218	3630 ± 272

[a]I_{max} and E_{max} values are expressed as fold change relative to baseline.
[b]SD of parameter estimate.

from the pooled data for renal and ileal CYP24A1 were summed to provide the total E_{max}; the EC_{50} was estimated as the average of the EC_{50} values for renal and intestinal CYP24A1.

Fitting of the PD-linked model to 1,25(OH)$_2$D$_3$ concentrations

Owing to the dose discrepancy and progressive changes that occur for R_{syn} and k_{10} with dose (Table 2), there was a need to incorporate the PD changes of CYP27B1 and CYP24A1 into the two-compartment model shown in Figure 1A (Appendix B). Hence, a PD-linked model (Figure 1B) was developed using scaled k_{12} values for greater doses. From fitting with data from the first doses, the EC_{50} (average of renal and ileal CYP24A1 EC_{50}) and the summed E_{max} for the kidney and intestine were used as initial estimates. Additionally, scaling factors and Hill coefficients for the inhibition and induction functions were added stepwise to monitor improvement of fit in order to determine the best predictive model. For data from the single doses, forced fitting with the PD-linked model showed significant improvement compared with the simple two-compartment model (Figure 5A and Table 4). The best outcome was obtained when all of these modifications were incorporated into the model (Table 4). Values of the Hill coefficients were close to unity, R_{syn} was 61.5 ± 5.24 fmol·h^{-1} (a value lower than that estimated from the two-compartment model), V_1 was similar to plasma volume and k_{10} [representing the basal elimination rate constant of 1,25(OH)$_2$D$_3$] was 0.128 ± 0.021 h^{-1}, a value lower than but reasonable to that estimated from the simple two-compartment model.

For fitting of data from all doses (Table 4), we further adopted a second strategy as there were changes in the EC_{50} upon repeated dosing. We used one EC_{50} [obtained from regression of FC vs. 1,25(OH)$_2$D$_3$ plasma concentrations from the first dose] or two different EC_{50} values [$EC_{50(1)}$ from regression of data from first dose and $EC_{50(2)}$ from pooled data]. When using one EC_{50}, it was assumed that the EC_{50} for the first dose was identical to that for the second and third doses and the regressed value from data from the first dose was used as the initial estimate. When using different EC_{50} values, $EC_{50(1)}$ obtained from the first dose and $EC_{50(2)}$ from pooled data were used as initial estimates. These EC_{50} values, together with scaled k_{12} functions, scaling factors and/or Hill coefficients in the PD-linked model, were incorporated in a stepwise manner for fitting (data not shown). From fits based on one or two EC_{50} values, we found that the parameters (k_{12}, k_{21}, k_{10}, V_1 and R_{syn}) and the scaling factors remained similar. The Hill coefficients using two EC_{50} values remained similar to unity, whereas those for the one EC_{50} model were greater (Table 4). Overall, it was concluded that the best fit was attained when all of these modifications, including different EC_{50} values, were added to the PD-linked model (Table 4). We also used parameters obtained from the 2 pmol first dose to simulate plasma 1,25(OH)$_2$D$_3$ concentration time data for other single and repeated dosing regimens, with use of one EC_{50} (Figure 5C) or two different EC_{50}s (Figure 5E). The simulations predicted the first dose reasonably well, but were unable to fully capture the later concentrations upon repeated dosing, presumably due to tolerance.

Indirect response model with inhibition and induction functions to explain 1,25(OH)$_2$D$_3$ PK

The PD components of the indirect response model incorporate both an indirect inhibitory (CYP27B1) and stimulatory (CYP24A1) response model. We added transit compartments with lag time (τ) to explain the time delay for CYP27B1 effects, as CYP27B1 was indirectly affected by vitamin D receptor activation by PTH (Figure 1C). A zero-order rate constant for formation (k_{in}), a first-order decay rate constant (k_{out}) and the appropriate inhibition and induction functions were added to account for decreased CYP27B1 and increased CYP24A1 production (Appendix C; Dayneka *et al.*, 1993; Sharma and Jusko, 1996). Preliminary fits showed that two additional transit compartments were needed to improve model fitting (data not shown). Improved fits were obtained when scaling factors and Hill coefficients were incorporated into the model. For the single dose data, the fitted parameter values for k_{12}, k_{21}, k_{10}, V_1 and R_{syn} were usually within twofold (Table 4). For the pooled data, when different EC_{50} values were used, greater values for k_{12} and $EC_{50(1)}$ values were obtained, whereas R_{syn} and the scaling factors were smaller (Table 4). Model fitting criteria were not statistically improved compared with the two-compartment model, although the indirect response model was able to reveal correlations between PD responses to 1,25(OH)$_2$D$_3$ concentrations in a temporal fashion (Figure 6).

Comparison of the two-compartment, PD-linked and indirect response models

Fitting of the two-compartment model to individual data sets revealed dose-dependent kinetics and reasonably good fits (Figure 2). However, fitting with the PD-linked model for the single dose data proved to be superior (Figure 5; Table 4). For repeated dosing, we found that the PD-linked model with different EC_{50} values was associated with smaller WSSR values with a significant F-value compared with the two-compartment model ($P < 0.05$), despite the larger AIC (Figure 5D; Table 4). Furthermore, incorporation of scaled k_{12} constants, scaling factors and Hill coefficients into the PD-linked model improved model performance (data not shown). Although the indirect response model did not improve the fit statistically compared with the two-compartment model, the model showed reasonable utility and was adequate in predicting changes in the temporal PD profiles against 1,25(OH)$_2$D$_3$ concentrations at the different administered dose levels (Figure 6).

Discussion and conclusions

1,25(OH)$_2$D$_3$ is used extensively for the treatment of secondary hyperparathyroidism in uraemic patients (Slatopolsky *et al.*, 1984; Kimura *et al.*, 1991; Brandi *et al.*, 2002) and has demonstrated therapeutic potential for anticancer therapy (Hershberger *et al.*, 2002; Rassnick *et al.*, 2008; Ramnath *et al.*, 2013). The therapeutic use of 1,25(OH)$_2$D$_3$ is often limited by the propensity of 1,25(OH)$_2$D$_3$ to cause hypercalcaemia and adverse effects. Recent studies have suggested that

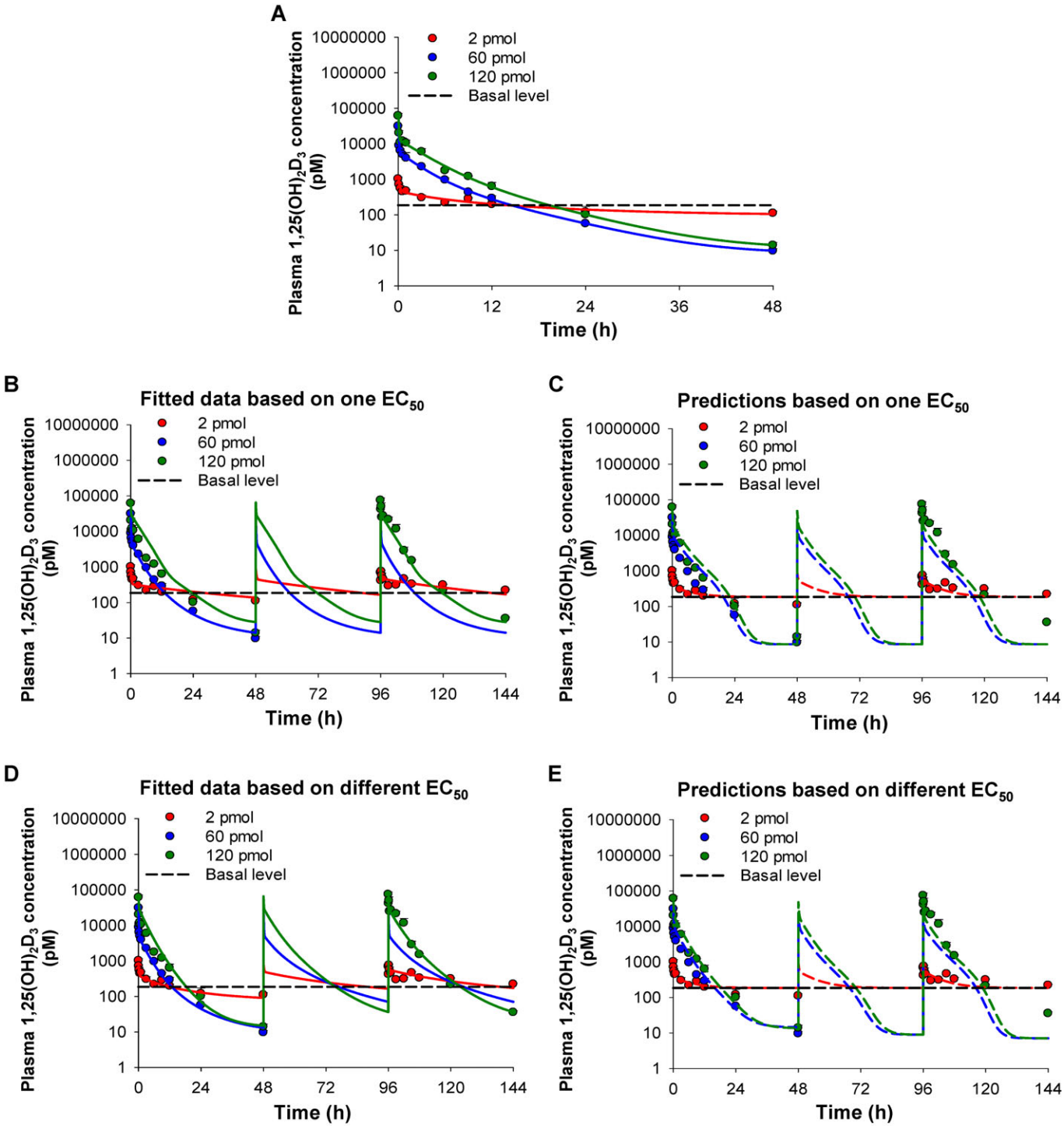

Figure 5

Fitting of single and repeated dose plasma $1,25(OH)_2D_3$ data using a PD-linked model. (A) Simultaneous fitting of single dose plasma $1,25(OH)_2D_3$ data. Simultaneous fitting of combined single and repeated dose plasma $1,25(OH)_2D_3$ using (B) one EC_{50} and (C) simulations to predict data for higher doses using parameters from the 2 pmol dose. Simultaneous fitting with (D) different EC_{50}s and (E) simulations to predict data for higher doses. Observed plasma $1,25(OH)_2D_3$ concentrations are shown as mean ± SEM (n = 3–4 different mice) with fitted values shown as a solid line and simulated values shown as a dashed line. Data for vehicle-treated mice (basal level) were averaged and joined by the dashed line (n = 9).

Table 4

Simultaneous fitting of first dose or pooled first and third dose data to different models with k_{12} scaled

	Combined fit to data of first dose			Combined fit to data of all doses (first and repeated third dose)			
Fitted parameters	**Two-compartment model**	**PD-linked model**	**Indirect response model**	**Two-compartment model**	**PD-linked model (one EC_{50})**	**PD-linked model (different EC_{50})**	**Indirect response model**
k_{12} (h^{-1})[a]	4.15 ± 1.23[d]	4.71 ± 2.22	3.88 ± 3.52	3.23 ± 0.77	2.75 ± 1.42	2.74 ± 1.34	6.17 ± 4.81
k_{21} (h^{-1})	1.89 ± 0.49	3.01 ± 0.24	1.70 ± 1.21	2.22 ± 0.55	2.83 ± 1.40	3.25 ± 1.42	3.75 ± 2.68
k_{10} (h^{-1})	0.75 ± 0.37	0.128 ± 0.021	0.349 ± 0.096	0.55 ± 0.27	0.091 ± 0.034	0.092 ± 0.007	0.133 ± 0.118
V_1 (mL)	2.33 ± 0.21	1.38 ± 0.30	1.79 ± 0.55	2.43 ± 0.31	1.86 ± 0.49	1.86 ± 0.49	1.43 ± 0.83
R_{syn} (fmol·h^{-1})	81.6 ± 16.4	61.5 ± 5.24	49.1 ± 9.2	78.9 ± 42.8	47.2 ± 16.1	44.5 ± 6.47	29.4 ± 19.0
E_{max}		398 ± 54.6	802 ± 175		404 ± 80.7	407 ± 47.4	1050 ± 515
$EC_{50(1)}$ (pM)		713 ± 137	1530 ± 1280		790 ± 248	616 ± 296	3110 ± 2990
$EC_{50(2)}$ (pM)						3810 ± 326	4640 ± 6110
I_{max}		11.3 ± 3.30	23.4 ± 5.41		11.6 ± 2.56	10.0 ± 3.07	45.2 ± 14.6
IC_{50} (pM)		276 ± 91.0	143 ± 218		306 ± 49.7	310 ± 74.8	388 ± 701
SM_1		4.24 ± 0.42	4.47 ± 0.87		5.41 ± 0.81	7.15 ± 1.38	0.81 ± 0.52
SM_2		25.8 ± 2.87	75.4 ± 16.6		25.9 ± 4.66	26.8 ± 6.20	9.64 ± 10.4
γ_1		1.25 ± 0.44	2.80 ± 0.96		1.85 ± 1.82	0.783 ± 0.391	2.12 ± 0.49
γ_2		0.983 ± 0.249	2.14 ± 0.21		1.33 ± 0.16	1.15 ± 0.154	2.50 ± 0.53
k_{in1} (h^{-1})[bc]			0.390 ± 0.163				0.343 ± 0.083
k_{in2} (h^{-1})[bc]			0.195 ± 0.110				0.362 ± 0.175
τ (h)			0.809 ± 0.114				1.36 ± 1.07
WSSR	5.73	0.47	709	30.2	23.6	11.8	676
AIC	523	649	982	913	1067	1086	1547
F-test value		28.3*	–1.53		1.48	7.09*	–1.32
$F_{critical}$ (df_1, df_2)		2.45 (8, 20)	2.41 (11, 17)		2.17 (8, 42)	2.12 (9, 41)	2.43 (12, 16)

[a]Values of k_{12} for the 60 and 120 pmol doses were assigned as 1.5× and 5.7× the value of k_{12} for the 2 pmol dose.
[b]k_{in1} and k_{in2} are the zero-order synthesis rate constants for CYP27B1 and CYP24A1, respectively.
[c]k_{out1} and k_{out2} are the first-order degradation rate constants for CYP27B1 and CYP24A1, respectively, and are equal to k_{in1} × baseline or k_{in2} × baseline, where baseline is 1.
[d]SD of parameter estimate.
*Significant difference between PD-linked versus two-compartment model at $P < 0.05$ compared with $F_{critical}$.

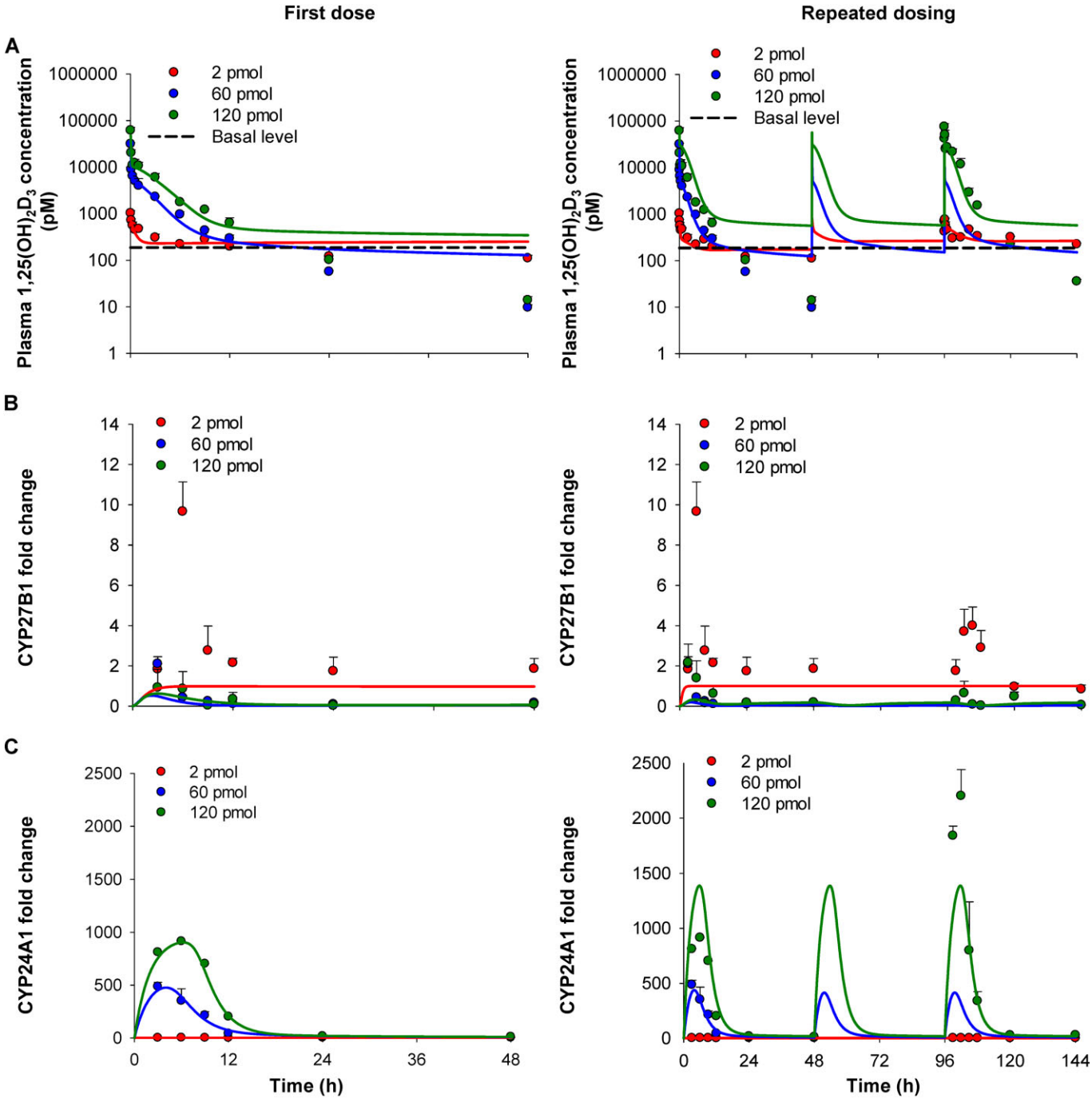

Figure 6

The indirect response model for simultaneous fitting of all data on plasma $1,25(OH)_2D_3$ and FC of vitamin D receptor target genes, CYP27B1 and CYP24A1. (A) Simultaneous fitting of single dose (left) and single and repeated dose (right) plasma $1,25(OH)_2D_3$ concentration. Simultaneous fitting for (B) inhibition of CYP27B1 FC and (C) stimulation of CYP24A1 FC. Observed plasma $1,25(OH)_2D_3$ concentrations and CYP27B1 and CYP24A1 FC are shown as mean ± SEM (n = 3–4 different mice) with fitted values shown as a solid line. Data for vehicle-treated mice (basal level) were averaged and joined by the dashed line (n = 9).

$1,25(OH)_2D_3$ may also play a beneficial role in lowering cholesterol (Chow *et al.*, 2014) as well as enhancement of amyloid-β efflux and reduction of cerebral plaque in transgenic mice expressing the human amyloid-β precursor protein (Durk *et al.*, 2014). Thus, an understanding of the PK and PD of $1,25(OH)_2D_3$ is critical for the prediction of a proper dose and dosing regimen for potential therapeutic uses.

Information on the PK of $1,25(OH)_2D_3$ is equivocal. Some of the discrepancies in the reported PK parameters of

1,25(OH)$_2$D$_3$ may exist due to species differences, inadequate sampling or dose-dependent PK and altered PD with dose and route. An examination of available literature regarding the PK properties of 1,25(OH)$_2$D$_3$ shows substantially different $t_{1/2}$ values with respect to dose and route of administration among species. In humans, a 4 μg dose of 1,25(OH)$_2$D$_3$ administered i.v. or p.o. resulted in a $t_{1/2}$ of 25.9 and 28.2 h, respectively (Brandi *et al.*, 2002), whereas a similar i.v. dose of 0.06 μg·kg^{-1} led to a shorter $t_{1/2}$ of 16.5 h (Salusky *et al.*, 1990). An equal dose of 20 μg·kg^{-1} administered i.p. and p.o. to the rat resulted in different $t_{1/2}$ values of 5.0 and 10.4 h (Vieth *et al.*, 1990). Administration of 10 and 50 μg·kg^{-1} of 1,25(OH)$_2$D$_3$ i.v. resulted in $t_{1/2}$ of 3.8 and 2.3 h respectively (Kissmeyer and Binderup, 1991). These shorter $t_{1/2}$ values are due to greater clearances and are the consequence of a greater induction of CYP24A1. In contrast, mice treated with single doses of 0.125 or 0.5 μg of 1,25(OH)$_2$D$_3$/mouse i.p. did not exhibit a clear dose-dependency, with $t_{1/2}$ of 7.6 and 7.8 h (Muindi *et al.*, 2004). Chow *et al.* (2013) also reported a $t_{1/2}$ of 6.8 h in mice treated i.p. with repeated doses of 0.05 μg per mouse 1,25(OH)$_2$D$_3$.

Our present study with 2, 60 and 120 pmol (0.00083, 0.025 and 0.05 μg per mouse) 1,25(OH)$_2$D$_3$ doses revealed dose-dependent $t_{1/2\beta}$ values ranging from 36.7 to 6.6 h (Table 1). Accordingly, CL_{total} values of 0.1, 2.0 and 1.8 mL·min^{-1}·kg^{-1} for 2, 60 and 120 pmol doses of 1,25(OH)$_2$D$_3$ were found (Table 1). Changes in enzymes were virtually absent for the 2 pmol dose, rendering the fitted parameters according to the two-compartment model pertinent to basal conditions, whereas maximal inhibitory (CYP27B1) and stimulatory (CYP24A1) responses were observed for the higher doses. Important information was revealed from fitted results from the lowest dose. For example, the volume of distribution of 1,25(OH)$_2$D$_3$ was low and R_{syn} was 71.9 ± 39.8 fmol·h^{-1}, a basal value that is higher than that (49.6 fmol·h^{-1}) previously reported by Hsu *et al.* (1987). Both the 60 and 120 pmol doses produced greater CL_{total} values (2.0 and 1.8 mL·min^{-1}·kg^{-1}) that were similar to i.p. mouse studies, with apparent CL_{total} values (CL_{total}/F where F is bioavailability of i.p. dose) of 1.2 and 2.8 mL·min^{-1}·kg^{-1}, estimated graphically from the data of Muindi *et al.* (2004), for doses of 0.125 and 0.5 μg per mouse.

Gene profiling of CYP27B1 and CYP24A1 in the kidney and intestine, two major vitamin D receptor-containing tissues, confirmed the inhibition and induction associated with 1,25(OH)$_2$D$_3$ administration (Figure 3). The dose-dependent down-regulation of renal CYP27B1 mRNA expression readily explains the decreased R_{syn} of 1,25(OH)$_2$D$_3$ for higher doses. Moreover, a dose-dependent induction of renal and ileal CYP24A1 mRNA expression further explains the increased CL_{total} and decreased $t_{1/2}$ with increasing dose. Interestingly, the concentration-response curve for CYP24A1 suggests tolerance as EC_{50} values were increased in mice given repeated doses of 1,25(OH)$_2$D$_3$ without a change in E_{max} (Figure 4). The observed tolerance may be attributed to a decreased binding affinity of 1,25(OH)$_2$D$_3$ to the vitamin D receptor. We also observed a sustained induction of renal CYP24A1 mRNA expression at 48 h, whereas ileal CYP24A1 expression returned to basal levels by 24 h post-injection for both single and repeated dosing. Long-term treatment with 1,25(OH)$_2$D$_3$ has been shown to lower CYP24A1 mRNA expression, suggesting a lack of activation of vitamin D receptor upon repeated dosing (unpublished data). Accordingly, the change in intestinal CYP24A1 mRNA level in response to 1,25(OH)$_2$D$_3$ has been described to be more short-lived than in kidney and becomes refractory to the continued administration of 1,25(OH)$_2$D$_3$, suggesting the presence of intestinal adaptation mechanisms which down-regulate the responsiveness of the enzyme (Lemay *et al.*, 1995). The sustained induction of renal, and not intestinal CYP24A1, and the fact that little to no intestinal removal occurs for systemically administered compounds (due to shunting of intestinal flow away from the enterocyte region) (Doherty and Pang, 1997; Cong *et al.*, 2000) suggest that renal CYP24A1 is the major enzyme for the catabolism of 1,25(OH)$_2$D$_3$ given i.v. Collectively, tolerance of CYP24A1 to repeated 1,25(OH)$_2$D$_3$ administration explains the inconsistency of the parameters derived from the PD-linked model for the 2 pmol dose in predicting 1,25(OH)$_2$D$_3$ profiles for higher doses and upon repeated dosing.

The present comprehensive analysis of 1,25(OH)$_2$D$_3$ quantification, together with gene profiling and data fitting using PD-linked and indirect response models, brings a new perspective as to how 1,25(OH)$_2$D$_3$ levels affect vitamin D receptor target genes and how these PD changes affect the PK of exogenously administered 1,25(OH)$_2$D$_3$. We recommend that PK studies involving 1,25(OH)$_2$D$_3$ incorporate PD effects and R_{syn} in order to fully capture the disposition of 1,25(OH)$_2$D$_3$. Changes in CYP27B1 and CYP24A1 expression alter the synthesis and degradation of 1,25(OH)$_2$D$_3$, and these events can be explained with appropriate PKPD models. By incorporating the PD changes, we were able to integrate the gene changes that affect 1,25(OH)$_2$D$_3$ concentrations, showing the mutual interaction of kinetics and dynamics. With our findings, we caution against merely reporting $t_{1/2}$, especially when the data do not cover the time course describing the decay. Our findings could explain the array of reported $t_{1/2}$ with different doses in the literature, as we show that clearance is dose-dependent and that CYP27B1 and CYP24A1 work closely to affect 1,25(OH)$_2$D$_3$ levels and *vice versa*. Clearly, the simple two-compartment model, although adequately showing dose-dependency for k_{12}, V_{ss}, R_{syn} and CL_{total}, could not fully explain the intricacies of the dose-dependent PK of 1,25(OH)$_2$D$_3$. Using the derived parameters of E_{max}, EC_{50}, I_{max} and IC_{50}, with or without incorporating changes in EC_{50} for single and repeated doses, we could adequately predict the dose-dependent PKPD profiles of 1,25(OH)$_2$D$_3$. Further modifications to the model, including scaled k_{12}, scaling factors and Hill coefficients significantly improved model performance. Although there is no apparent improvement with the indirect response model statistically, we could demonstrate the direct correlation between 1,25(OH)$_2$D$_3$ and vitamin D receptor target genes and essential time delays using transit compartments in the model (Mager and Jusko, 2001; Mager *et al.*, 2003).

The unique PK of exogenously administered 1,25(OH)$_2$D$_3$ rests on the inhibition and induction of its own synthesis and metabolism, although there has been other evidence for altered 1,25(OH)$_2$D$_3$ efficacy due to single nucleotide polymorphisms in the CYP24A1 gene (Chen *et al.*, 2011; Ramnath *et al.*, 2013). We have demonstrated that future studies involving the administration of 1,25(OH)$_2$D$_3$ as a therapeutic

agent should incorporate R_{syn} and PD effects of CYP27B1 and CYP24A1 in order to fully explain the disposition of $1,25(OH)_2D_3$ in the body. This present investigation on the PKPD relationships with respect to renal and intestinal handling of synthesis and metabolism via down-regulation of CYP27B1 and induction of CYP24A1 has expanded ways to view changes of other vitamin D receptor target genes and their PD effects. A physiologically based PKPD model could extend this model to different routes of administration to describe the regulatory effects of the vitamin D receptor on vitamin D receptor target genes in other tissues in the body.

Acknowledgements

We thank Dr. Matthew R. Durk for assistance in the study. This work was supported by the Canadian Institutes of Health Research (K. S. P.), the National Sciences and Engineering Research Council of Canada (H. P. Q. and E. C. C.) and the Ontario Graduate Scholarship Program (H. P. Q.).

Author contributions

H. P. Q., E. C. C. and S. Y. H. performed the experiments. H. P. Q., E. C. C. and K. S. P. designed the research study. H. P. Q., Q. J. Y., D. E. M. and K. S. P. analysed the data and wrote the manuscript. H. P. Q., E. C. C. and K. S. P. revised the manuscript.

Conflicts of interest

None.

References

Akeno N, Saikatsu S, Kimura S, Horiuchi N (1994). Induction of vitamin D 24-hydroxylase messenger RNA and activity by 22-oxacalcitriol in mouse kidney and duodenum. Possible role in decrease of plasma 1α,25-dihydroxyvitamin D_3. Biochem Pharmacol 48: 2081–2090

Alexander SPH, Benson HE, Faccenda E, Pawson AJ, Sharman JL, Spedding M *et al*. (2013a). The Concise Guide to PHARMACOLOGY 2013/14: ion channels. Br J Pharmacol 170: 1607–1651.

Alexander SPH, Benson HE, Faccenda E, Pawson AJ, Sharman JL, Spedding M *et al*. (2013b). The Concise Guide to PHARMACOLOGY 2013/14: nuclear hormone receptors. Br J Pharmacol 170: 1652–1675.

Alexander SPH, Benson HE, Faccenda E, Pawson AJ, Sharman JL, Spedding M *et al*. (2013c). The Concise Guide to PHARMACOLOGY 2013/14: enzymes. Br J Pharmacol 170: 1797–1867.

Boxenbaum HG, Riegelman S, Elashoff RM (1974). Statistical estimations in pharmacokinetics. J Pharmacokinet Biopharm 2: 123–148.

Brandi L, Egfjord M, Olgaard K (2002). Pharmacokinetics of $1,25(OH)_2D_3$ and $1\alpha(OH)D_3$ in normal and uraemic men. Nephrol Dial Transplant 17: 829–842.

Brenza HL, DeLuca HF (2000). Regulation of 25-hydroxyvitamin D_3 1α-hydroxylase gene expression by parathyroid hormone and 1,25-dihydroxyvitamin D_3. Arch Biochem Biophys 381: 143–152.

Carrillo-Lopez N, Alvarez-Hernandez D, Gonzalez-Suarez I, Roman-Garcia P, Valdivielso JM, Fernandez-Martin JL *et al*. (2008). Simultaneous changes in the calcium-sensing receptor and the vitamin D receptor under the influence of calcium and calcitriol. Nephrol Dial Transplant 23: 3479–3484.

Chen G, Kim SH, King AN, Zhao L, Simpson RU, Christensen PJ *et al*. (2011). CYP24A1 is an independent prognostic marker of survival in patients with lung adenocarcinoma. Clin Cancer Res 17: 817–826.

Chow EC, Maeng HJ, Liu S, Khan AA, Groothuis GM, Pang KS (2009). 1α,25-Dihydroxyvitamin D_3 triggered vitamin D receptor and farnesoid X receptor-like effects in rat intestine and liver *in vivo*. Biopharm Drug Dispos 30: 457–475.

Chow EC, Durk MR, Cummins CL, Pang KS (2011). 1α,25-dihydroxyvitamin D_3 up-regulates P-glycoprotein via the vitamin D receptor and not farnesoid X receptor in both *fxr(–/–)* and *fxr(+/+)* mice and increased renal and brain efflux of digoxin in mice *in vivo*. J Pharmacol Exp Ther 337: 846–859.

Chow EC, Quach HP, Vieth R, Pang KS (2013). Temporal changes in tissue 1α,25-dihydroxyvitamin D_3, vitamin D receptor target genes, and calcium and PTH levels after $1,25(OH)_2D_3$ treatment in mice. Am J Physiol Endocrinol Metab 304: E977–E989.

Chow EC, Magomedova L, Quach HP, Patel R, Durk MR, Fan J *et al*. (2014). Vitamin D receptor activation down-regulates the small heterodimer partner and increases CYP7A1 to lower cholesterol. Gastroenterology 146: 1048–1059.

Chun RF (2012). New perspectives on the vitamin D binding protein. Cell Biochem Funct 30: 445–456.

Clements MR, Davies M, Hayes ME, Hickey CD, Lumb GA, Mawer EB *et al*. (1992). The role of 1,25-dihydroxyvitamin D in the mechanism of acquired vitamin D deficiency. Clin Endocrinol 37: 17–27.

Cong D, Doherty M, Pang KS (2000). A new physiologically based, segregated-flow model to explain route-dependent intestinal metabolism. Drug Metab Dispos 28: 224–235.

Dayneka NL, Garg V, Jusko WJ (1993). Comparison of four basic models of indirect pharmacodynamic responses. J Pharmacokinet Biopharm 21: 457–478.

den Dekker E, Hoenderop JG, Nilius B, Bindels RJ (2003). The epithelial calcium channels, TRPV5 & TRPV6: from identification towards regulation. Cell Calcium 33: 497–507.

Doherty MM, Pang KS (1997). First-pass effect: significance of the intestine for absorption and metabolism. Drug Chem Toxicol 20: 329–344.

Durk MR, Han K, Chow EC, Ahrens R, Henderson JT, Fraser PE *et al*. (2014). 1α,25-Dihydroxyvitamin D_3 reduces cerebral amyloid-β accumulation and improves cognition in mouse models of Alzheimer's disease. J Neurosci 34: 7091–7101.

Halloran BP, Castro ME (1989). Vitamin D kinetics *in vivo*: effect of 1,25-dihydroxyvitamin D administration. Am J Physiol 256: E686–E691.

Henry HL (2001). The 25(OH)D$_3$/1α,25(OH)$_2$D$_3$-24R-hydroxylase: a catabolic or biosynthetic enzyme? Steroids 66: 391–398.

Hershberger PA, McGuire TF, Yu WD, Zuhowski EG, Schellens JH, Egorin MJ *et al*. (2002). Cisplatin potentiates 1,25-dihydroxyvitamin D$_3$-induced apoptosis in association with increased mitogen-activated protein kinase kinase kinase 1 (MEKK-1) expression. Mol Cancer Ther 1: 821–829.

Hoenderop JG, Nilius B, Bindels RJ (2005). Calcium absorption across epithelia. Physiol Rev 85: 373–422.

Holick MF, Schnoes HK, DeLuca HF, Gray RW, Boyle IT, Suda T (1972). Isolation and identification of 24,25-dihydroxycholecalciferol, a metabolite of vitamin D made in the kidney. Biochemistry 11: 4251–4255.

Hsu CH, Patel S, Young EW, Simpson RU (1987). Production and degradation of calcitriol in renal failure rats. Am J Physiol 253: F1015–F1019.

Jones G, Vriezen D, Lohnes D, Palda V, Edwards NS (1987). Side-chain hydroxylation of vitamin D$_3$ and its physiological implications. Steroids 49: 29–53.

Jones G, Strugnell SA, DeLuca HF (1998). Current understanding of the molecular actions of vitamin D. Physiol Rev 78: 1193–1231.

Kilkenny C, Browne W, Cuthill IC, Emerson M, Altman DG (2010). Animal research: reporting *in vivo* experiments: the ARRIVE guidelines. Br J Pharmacol 160: 1577–1579.

Kimura Y, Nakayama M, Kuriyama S, Watanabe S, Kawaguchi Y, Sakai O (1991). Pharmacokinetics of active vitamins D$_3$, 1α-hydroxyvitamin D$_3$ and 1α,25-dihydroxyvitamin D$_3$ in patients on chronic hemodialysis. Clin Nephrol 35: 72–77.

Kissmeyer AM, Binderup L (1991). Calcipotriol (MC 903): pharmacokinetics in rats and biological activities of metabolites. A comparative study with 1,25(OH)$_2$D$_3$. Biochem Pharmacol 41: 1601–1606.

Kumar R, Schnoes HK, DeLuca HF (1978). Rat intestinal 25-hydroxyvitamin D$_3$- and 1α,25-dihydroxyvitamin D$_3$-24-hydroxylase. J Biol Chem 253: 3804–3809.

Lemay J, Demers C, Hendy GN, Delvin EE, Gascon-Barre M (1995). Expression of the 1,25-dihydroxyvitamin D$_3$-24-hydroxylase gene in rat intestine: response to calcium, vitamin D$_3$ and calcitriol administration *in vivo*. J Bone Miner Res 10: 1148–1157.

Mager DE, Jusko WJ (2001). Pharmacodynamic modeling of time-dependent transduction systems. Clin Pharmacol Ther 70: 210–216.

Mager DE, Wyska E, Jusko WJ (2003). Diversity of mechanism-based pharmacodynamic models. Drug Metab Dispos 31: 510–518.

Mager DE, Woo S, Jusko WJ (2009). Scaling pharmacodynamics from in vitro and preclinical animal studies to humans. Drug Metab Pharmacokinet 24: 16–24.

Makin G, Lohnes D, Byford V, Ray R, Jones G (1989). Target cell metabolism of 1,25-dihydroxyvitamin D$_3$ to calcitroic acid. Evidence for a pathway in kidney and bone involving 24-oxidation. Biochem J 262: 173–180.

Masuda S, Byford V, Arabian A, Sakai Y, Demay MB, St-Arnaud R *et al*. (2005). Altered pharmacokinetics of 1α,25-dihydroxyvitamin D$_3$ and 25-hydroxyvitamin D$_3$ in the blood and tissues of the 25-hydroxyvitamin D-24-hydroxylase (Cyp24a1) null mouse. Endocrinology 146: 825–834.

McGrath J, Drummond G, McLachlan E, Kilkenny C, Wainwright C (2010). Guidelines for reporting experiments involving animals: the ARRIVE guidelines. Br J Pharmacol 160: 1573–1576.

Muindi JR, Modzelewski RA, Peng Y, Trump DL, Johnson CS (2004). Pharmacokinetics of 1α,25-dihydroxyvitamin D$_3$ in normal mice after systemic exposure to effective and safe antitumor doses. Oncology 66: 62–66.

Pawson AJ, Sharman JL, Benson HE, Faccenda E, Alexander SP, Buneman OP *et al*.; NC-IUPHAR (2014). The IUPHAR/BPS Guide to PHARMACOLOGY: an expert-driven knowledgebase of drug targets and their ligands. Nucl Acids Res 42 (Database Issue): D1098–D1106.

Ramnath N, Daignault-Newton S, Dy GK, Muindi JR, Adjei A, Elingrod VL *et al*. (2013). A phase I/II pharmacokinetic and pharmacogenomic study of calcitriol in combination with cisplatin and docetaxel in advanced non-small-cell lung cancer. Cancer Chemother Pharmacol 71: 1173–1182.

Rassnick KM, Muindi JR, Johnson CS, Balkman CE, Ramnath N, Yu WD *et al*. (2008). *In vitro* and *in vivo* evaluation of combined calcitriol and cisplatin in dogs with spontaneously occurring tumors. Cancer Chemother Pharmacol 62: 881–891.

Salusky IB, Goodman WG, Horst R, Segre GV, Kim L, Norris KC *et al*. (1990). Pharmacokinetics of calcitriol in continuous ambulatory and cycling peritoneal dialysis patients. Am J Kidney Dis 16: 126–132.

Sharma A, Jusko WJ (1996). Characterization of four basic models of indirect pharmacodynamic responses. J Pharmacokinet Biopharm 24: 611–635.

Shinki T, Jin CH, Nishimura A, Nagai Y, Ohyama Y, Noshiro M *et al*. (1992). Parathyroid hormone inhibits 25-hydroxyvitamin D$_3$-24-hydroxylase mRNA expression stimulated by 1α,25-dihydroxyvitamin D$_3$ in rat kidney but not in intestine. J Biol Chem 267: 13757–13762.

Slatopolsky E, Weerts C, Thielan J, Horst R, Harter H, Martin KJ (1984). Marked suppression of secondary hyperparathyroidism by intravenous administration of 1,25-dihydroxy-cholecalciferol in uremic patients. J Clin Invest 74: 2136–2143.

Smith DC, Johnson CS, Freeman CC, Muindi J, Wilson JW, Trump DL (1999). A phase I trial of calcitriol (1,25-dihydroxycholecalciferol) in patients with advanced malignancy. Clin Cancer Res 5: 1339–1345.

Turunen MM, Dunlop TW, Carlberg C, Vaisanen S (2007). Selective use of multiple vitamin D response elements underlies the 1α,25-dihydroxyvitamin D$_3$-mediated negative regulation of the human CYP27B1 gene. Nucleic Acids Res 35: 2734–2747.

Vieth R, Kooh SW, Balfe JW, Rawlins M, Tinmouth WW (1990). Tracer kinetics and actions of oral and intraperitoneal 1,25-dihydroxyvitamin D$_3$ administration in rats. Kidney Int 38: 857–861.

Supporting information

Additional Supporting Information may be found in the online version of this article at the publisher's web-site:

http://dx.doi.org/10.1111/bph.13153

Figure S1 Weighted sum of squares residuals versus time plots for the (A) two-compartment and (B) PD-linked models. The dashed line represents y = 0.

Appendix A

For the simple two-compartment model (Figure 1A):

$$V_1 \frac{dC_1}{dt} = R_{syn} - k_{12}C_1V_1 + k_{21}A_2 - k_{10}C_1V_1 \quad (A1)$$

$$\frac{dA_2}{dt} = k_{12}C_1V_1 - k_{21}A_2 \quad (A2)$$

Note: k_{12} for the 60 pmol dose is 1.5× k_{12} of the 2 pmol dose; k_{12} for the 120 pmol dose is 5.7× k_{12} of the 2 pmol dose.

Appendix B

For PD-linked model with scaling factors (SM_1 and SM_2) and Hill coefficients (γ_1 and γ_2) (Figure 1B)

$$V_1 \frac{dC_1}{dt} = R_{syn} \frac{\left(1 - \frac{I_{max}C_1^{\gamma_1}}{IC_{50}^{\gamma_1} + C_1^{\gamma_1}}\right)}{SM_1} - k_{12}C_1V_1 + k_{21}A_2 - \mathbf{k}_{10}C_1V_1 \frac{\left(1 + \frac{\sum E_{max}C_1^{\gamma_2}}{EC_{50}^{\gamma_2} + C_1^{\gamma_2}}\right)}{SM_2} \quad (B1)$$

Appendix C

For the indirect response model, with scaling factors (SM_1 and SM_2) to adjust for fold changes (FC) (Figure 1C)

$$V_1 \frac{dC_1}{dt} = \frac{R_{syn} \times CYP27B1_{FC}}{SM_1} - k_{12}C_1V_1 + k_{21}A_2 - \frac{k_{10}C_1V_1 \times CYP24A1_{FC}}{SM_2} \quad (C1)$$

The rates of change in PD responses (CYP27B1 or CYP24A1) can be described as

$$\frac{dR}{dt} = k_{in} - k_{out} \times R \quad (C2)$$

where k_{in} is the zero-order rate constant for production of the response and k_{out} is the first-order rate constant for loss of the response. The response variable, R, in this study is the same as the FC of vitamin D receptor target gene mRNA expression. The inhibition (Equation 1) and induction (Equation 2) functions were included, respectively, to account for the inhibition of CYP27B1 and induction of CYP24A1. Inhibition of the CYP27B1 response variable ($k_{in}^{CYP27B1}$) and induction of the CYP24A1 response variable ($k_{in}^{CYP24A1}$) were described as

$$\frac{dCYP27B1_{FC}}{dt} = k_{in}^{CYP27B1} \times \left(1 - \frac{I_{max}C_p^{\gamma_1}}{IC_{50}^{\gamma_1} + C_p^{\gamma_1}}\right) - k_{out}^{CYP27B1} \times CYP27B1_{FC} \quad (C3)$$

$$\frac{dCYP24A1_{FC}}{dt} = k_{in}^{CYP24A1} \times \left(1 + \frac{E_{max}C_p^{\gamma_2}}{EC_{50}^{\gamma_2} + C_p^{\gamma_2}}\right) - k_{out}^{CYP24A1} \times CYP24A1_{FC} \quad (C4)$$

where C_p is the plasma 1,25(OH)2D3 concentration; $k_{in} = k_{out}$ × baseline, with baseline = 1; I_{max} and E_{max} are the maximal FC for inhibition and induction factors; and IC_{50} and EC_{50} are the plasma concentrations that result in 50% of I_{max} and E_{max}. The E_{max} is the sum of the E_{max} from the intestine and kidney.

A time-delay function was required to provide a better fit for CYP27B1 expression, where τ is the time delay in h and $A_{transit1}$ and $A_{transit2}$ are the amounts in transit compartments 1 and 2 respectively:

$$\frac{dA_{transit_1}}{dt} = \frac{CYP27B1_{FC} - A_{transit1}}{\tau} \quad (C5)$$

$$\frac{dA_{transit_2}}{dt} = \frac{A_{transit_2} - A_{transit_1}}{\tau} \quad (C6)$$